Enabling Logic Computation Between Ta/CoFeB/MgO Nanomagnets

Enabling Logic Computation Between Ta/CoFeB/MgO Nanomagnets

Diego Favaro[1], Luca Gnoli[1], Valentin Ahrens[2], Simon Mendisch[2], Marco Vacca[1], Giovanna Turvani[1], Markus Becherer[2], and Fabrizio Riente[1]

[1]Department of Electronics and Telecommunications, Politenico di Torino, 10129 Turin, Italy
[2]Nanomagnetic Devices Group, Chair of Nano and Quantum Sensors, Department of Electrical and Computer Engineering, Technical University of Munich, 80333 Munich, Germany

Dipolar coupled magnets proved to have the potential to be capable of successfully performing digital computation in a highly parallel way. For that, nanomagnet-based computation requires precise control of the domain wall nucleation from a well-localized region of the magnet. Co/Pt and Co/Ni multilayer stacks were successfully used to demonstrate a variety of computing devices. However, Ta/CoFeB/MgO appears more promising, thanks to the lower switching field required to achieve a full magnetization reversal, reduced thickness (less than 10 nm), and its compatibility with magnetic tunnel junctions. In this work, the switch of the information is achieved through the application of a magnetic field, which allows to scale more the nanomagnets with respect to current-driven magnetization reversal-based devices and to go toward 3-D structures. We experimentally demonstrate that Ga^+ ions can be used to tune the energy landscape of the structured magnets to provide signal directionality and achieve a distinct logic computation. We prove that it is possible to define the artificial nucleation center (ANC) in different structures with two irradiation steps and that this approach can enable logic computation in ultrathin films by dipolar interaction. Moreover, different from previous studies, the results coming from the irradiation analysis are then used for real logic devices. We present the experimental demonstration of a set of fully working planar inverters, showing that it is possible to reach a coupling field between the input and the output, which is strong enough to reliably implement logic operations. Micromagnetic simulations are used to study the nucleation center's effectiveness with respect to its position in the magnet and to support the experiments. Our results open the path to the development of more efficient nanomagnet-based logic circuits.

Index Terms— **Artificial nucleation, CoFeB\MgO, logic devices, nano magnetic logic, spintronic devices.**

I. Introduction

CoFeB/MgO thin films are becoming more and more attractive, thanks to their excellent magnetic and electric characteristics that promoted their broad use in spintronic technologies, such as magnetic tunnel junctions and nonvolatile memories [1], [2], [3], [4]. In particular, some logic applications require precise control of the domain wall nucleation and propagation direction [5]. So far, Co/Pt and Co/Ni multilayer stacks were the technology drivers of perpendicular nano magnetic logic (pNML) devices [6], [7], [8], [9]. Due to power constraints related to the high nucleation and depinning fields characteristic of the materials used so far for logic, Ta/CoFeB/MgO stacks appear a promising alternative to increase the efficiency in dipolar computations [10]. In field-coupled technologies, the binary information is encoded in the bistable magnetization state of the nanomagnets. Magnetostatic interactions between neighbor magnets are exploited to propagate information and perform logic computation. Logic gates and a variety of computing structures have been successfully demonstrated experimentally using Co/Pt and Co/Ni multilayer stacks [7], [11]. Those materials showed strong field coupling on inverters and majority gates. Recent works on the ion irradiation effects on CoFeB/MgO, and in particular Ta/CoFeB/MgO, show interesting results in controlling the domain nucleation and domain wall depinning fields [10], [12]. Both He^+ and Ga^+ ion irradiation were successfully used to tune the energy landscape of the material at film level [13]. Mendisch et al. [10] and Breitkreutz et al. [12] recently demonstrated that magnetic anisotropy can be lowered by ion irradiation at the film level and locally on structured nanomagnets. The possibility to tune the effective anisotropy makes the system extremely versatile and useful for the development of logic devices. In this article, we investigate the application of Ga^+ irradiation on patterned Ta/CoFeB/MgO for the realization of perpendicular nanomagnetic logic devices. The aim of this study is to demonstrate how Ta/CoFeB/MgO patterned structures locally tuned by means of Ga^+ focused ion beam (FIB) irradiation are able to generate enough dipolar coupling to perform logic computation. First, we analyze the effects of different ion doses on magnetic wires to identify a suitable dose to generate reliable artificial nucleation centers (ANCs). Second, the collected information about nucleation is used to produce nanomagnetic devices able to realize the inversion operation. The devices are finally analyzed in terms of the dipolar coupling between the inputs and outputs. The findings are supported by micromagnetic simulations that combined with atomic force microscope (AFM) measurements made possible the analysis of the effects of ANC positioning on the coupling in real devices.

Manuscript received 9 September 2022; revised 4 January 2023 and 27 February 2023; accepted 7 March 2023. Date of publication 10 March 2023; date of current version 25 April 2023. Corresponding author: F. Riente (e-mail: fabrizio.riente@polito.it).

Color versions of one or more figures available at https://doi.org/10.1109/TMAG.2023.3255306.

Digital Object Identifier 10.1109/TMAG.2023.3255306

II. Methods

A. Sample Preparation

The study presented in this article is based on a layered magnetic structure made of Ta(2)/$Co_{20}Fe_{60}B_{20}$(1.1)/MgO(2)/Ta(3) where the numbers in parenthesis represent the nominal nanometer thickness of the layers. The stack is deposited at room temperature via confocal RF-magnetron sputtering onto Si substrate (100), covered by a thermal oxide with a thickness of 50 nm. Each layer is deposited in Ar gas atmosphere at a constant working pressure of 4 μbar, except for the MgO layer that is deposited at 1 μbar. To obtain the requested perpendicular magnetic anisotropy (PMA), the sample is annealed after deposition in a N_2 atmosphere at 275 °C for 5 min. The deposited stack has been patterned via Ga^+ lithography using a 50 keV FIB oriented perpendicularly to the sample surface with a nominal spatial resolution of 10 nm. The patterning process consists of the deposition of a thin poly methyl methacrylate (PMMA) resist (≈50 nm) via spin coating. The resist is then irradiated with Ga^+ FIB following a computer-defined mask. After PMMA development, a thin Ti layer (≈5 nm) is evaporated as a hard mask, and the remaining resist is removed in a lift-off process. Only the structures defined by FIB lithography are covered by the Ti hard mask. Finally, the magnetic stack is structured by ion-beam etching, where Ar^+ ions are accelerated by an electric field of 250 eV. Areal and local Ga^+ ion irradiation are used to engineer the energy landscape of the structured Ta/CoFeB/MgO magnets and obtain the controlled nucleation required by dipolar coupled devices.

B. Measurement Setup

The characterization of the structured nanomagnets is carried out via Widefield Magneto-Optical Kerr microscopy (WMOKE) under the stimulus of a magnetic field perpendicular to the sample. The setup is used to study the switching behavior of the structures.

The measurements are performed by applying a sequence of magnetic field pulses in the millisecond regime generated by an electromagnet and observing the resulting magnetization state. To increase the contrast of the measurements, every observation is performed as a differential measure with respect to a reference image taken with the sample saturated in a predefined direction. Fig. 1 schematically depicts the adopted measurement methodology. As a first step, the nanomagnets are saturated and a reference image is taken. The switch of the nanomagnets is then evaluated after applying an external out-of-plane field. For each field value, many pulses are applied to estimate the distribution of the switching events. One image is collected after every field pulse.

III. Results and Discussion

To identify the Ga^+ ion doses required to generate the nucleation centers, the magnetic stack has been first patterned in nanowires with a length of 10 μm and a variable width ranging from 450 to 700 nm, with increments of 50 nm. In these structures, the nucleation centers are placed as close as possible to the left edge of the wire to maximize the ANC effect on the wire coercivity, as shown from the simulation reported in Appendix A. Fig. 2(a) shows the optical micrograph of the magnetic structures. The shown pattern has been replicated multiple times on the same sample to perform the studies over a range of doses, both for the mild areal irradiation and for the strong localized irradiation for ANC generation. On the same sample, planar inverters were also fabricated to evaluate the input–output coupling strength. The devices are visible in Fig. 2(b).

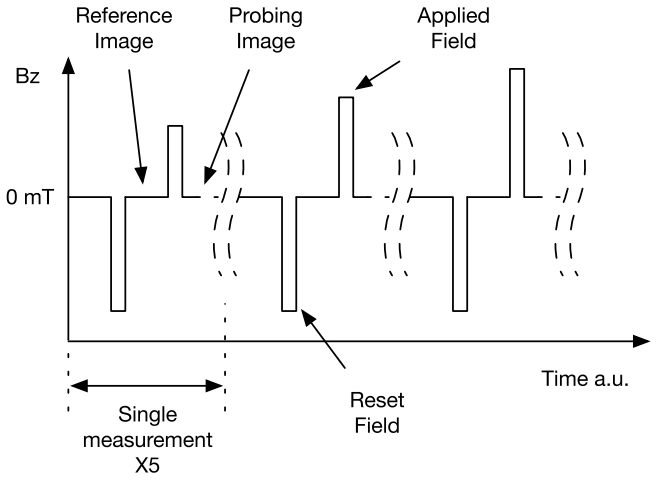

Fig. 1. Schematic representation of the measurement method used for the characterization of the nanomagnets.

A. Ion Dose Evaluation

To perform logic operations with nanomagnets, it is necessary to have control over the domain nucleation in the output magnet. Controlling the point of nucleation is essential to set the information propagation direction and maximize the effect of the magnetic coupling. This goal can be achieved by modifying the magnetic properties of the device by ion irradiation and diversifying the switching behavior of input and output magnets.

To achieve controlled and localized domain nucleation, we use a two-step irradiation scheme. First, an areal irradiation of the whole surface of the magnets is performed to increase the switching field and even out the anisotropy landscape [14] to create a better environment for ANC generation [2], [10]. Second, a small area of the magnet is irradiated to reduce the anisotropy locally and lower the switching field to produce an ANC. To optimize the ion dose for areal irradiation, the switching field of patterned magnetic wires, as shown in Fig. 2(a), is measured before and after irradiation. The switching field variation is computed as the difference between the switching field after irradiation and before irradiation. In Fig. 3, the switching field difference related to the 500 nm wires is shown as a function of the irradiation dose. For medium values ranging from around 1.5×10^{13} to 3×10^{13} ions/cm^2, a distinct increase in the switching field was measured, whereas low doses slightly decrease the switching field. Negative numbers indicate that a reduction of the switching field was observed with respect to the pristine case.

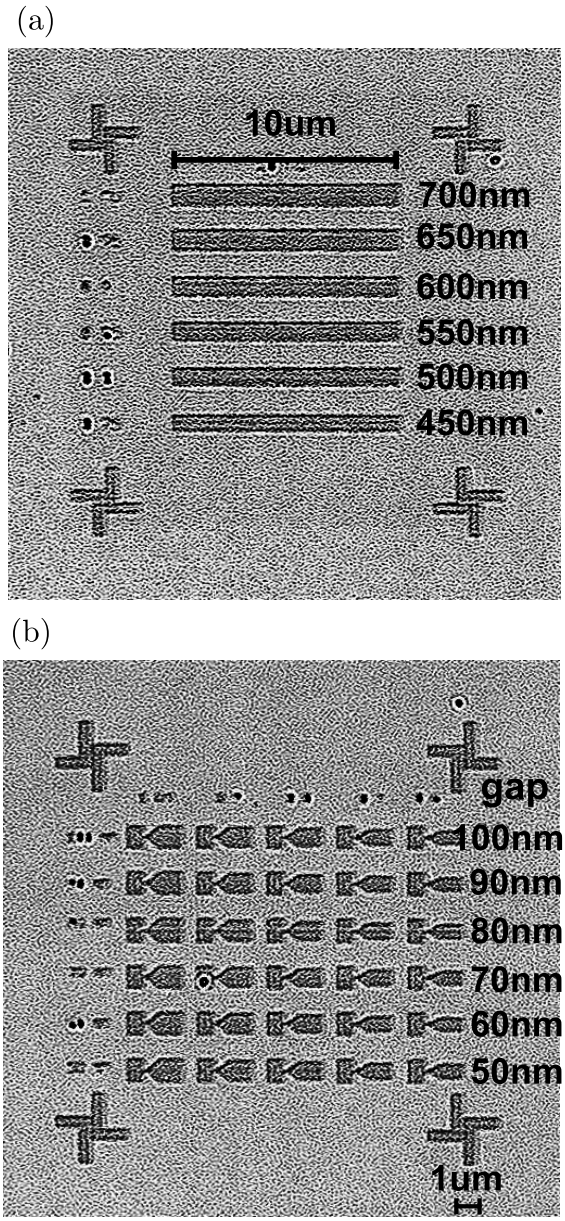

Fig. 2. Optical images of the structures considered in the study. (a) Wire array with different widths. (b) Array of inverters with different input–output gaps and different widths of the output magnet ranging from 1 μm (left) to 600 nm (right).

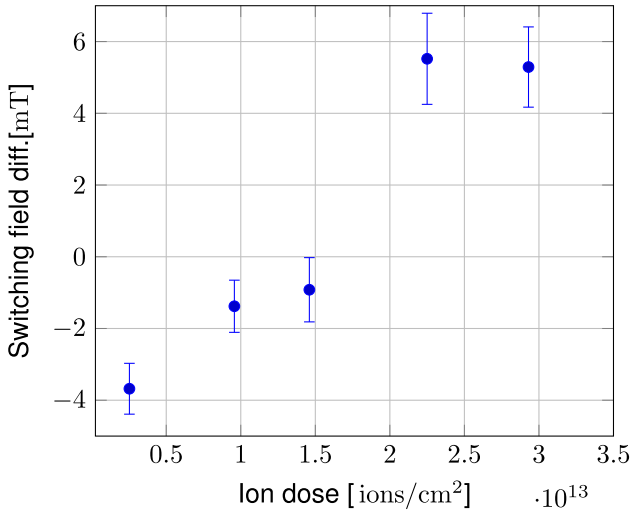

Fig. 3. Switching field difference of the 500 nm-wide magnetic wires with respect to the switching field value before irradiation. The values are computed as a difference between the switching field after areal irradiation and the pristine wire.

The trend shown in the experiment is in agreement with the results in [10] that explored the same kind of irradiation on magnetic dots and it is confirmed for all the tested wires. The increase in the switching field measured for medium ion doses is considered to be related to a rise in the effective magnetic anisotropy $K_{\text{eff}} = K_{\text{u}} - (\mu_0 M_s^2/2)$ where K_u represents the perpendicular uniaxial anisotropy of the systems and M_s is the saturation magnetization. This increment could derive from a reduction in K_u, a reduction in M_{sat}, or both the effects together. The ion doses exploited in this experiment are expected to induce at the interfaces of the ferromagnet the intermixing of atoms, modulating progressively the resulting magnetic properties [10], [12], [14], [15]. Mendisch et al. [10] demonstrated an initial reduction in the saturation magnetization after FIB irradiation with Ga^+ ions for low doses followed by an increase in the film anisotropy. This behavior is attributed to an intermix of Ta within the CoFeB layer as also discussed in [14], where the system was irradiated with He^+ ions. Tantalum is known to generate in contact with CoFeB, a large magnetic dead layer; the resulting CoFeTa alloy is characterized by a lower magnetization with respect to CoFeB. The same observations were made by Devolder et al. [13] where their system was irradiated with He^+ ions.

Mendisch et al. [10] demonstrated that in systems irradiated with Ga^+ ion doses beyond a certain limit, the coercivity is lowered with respect to the case of pristine magnets. This behavior, correlated with the ion dose, gives the possibility to produce by means of irradiation an ANC, enabling the control of the magnetization reversal. In this case, due to the high number of ions' collisions, the ferromagnet crystal structure grown after the annealing and the interfaces with the other materials composing the stack are modified, causing a visible change in the effective anisotropy. This change could also interest other magnetic parameters as already demonstrated with He^+ irradiation [12], [14], [15] and Ga^+ irradiation [10]. Nevertheless, the parameters mostly affecting the switching are expected to be the saturation magnetization and the interfacial anisotropy.

To obtain a local nucleation point on the patterned magnetic wires shown in Fig. 2, at first, the areal irradiation is performed with an ion dose of $\approx 2.25 \times 10^{13}$ ions/cm^2 on the whole surface. Second, a local irradiation step to define the ANC with higher doses is introduced. To find the optimal ion dose required for the generation of nucleation center, the switching field of patterned magnetic wires is measured before and after the ANC definition step. The ANC doses applied are varied from $\approx 6.9 \times 10^{13}$ to $\approx 9 \times 10^{13}$ ions/cm^2. The second irradiation step is performed in a square with sides of 250 nm, kept as close as possible to the edge of the wire.

In Fig. 4, the switching field difference in the wires of width 500 nm after areal and ANC irradiation are plotted over the

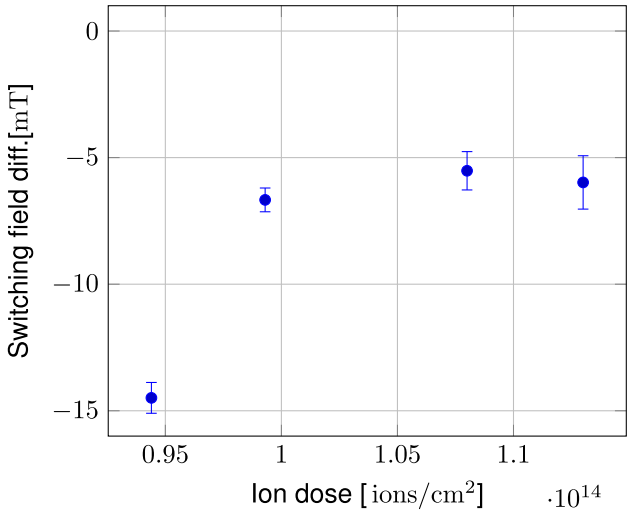

Fig. 4. Switching field difference of the 500 nm magnetic wires after areal and ANC irradiation plotted over the cumulative ion dose.

cumulative ion dose with respect to the pristine case. Those doses are the sum of the areal irradiation previously applied, 2.25×10^{13} ions/cm^2, and the local doses for the ANCs. From the obtained results, the lowest switching field observed is obtained with a cumulative ion dose of 9.44×10^{13} ions/cm^2. On the other hand, increasing the dose decreases this effect showing an increase in the switching field up to the highest dose investigated (1.13×10^{14} ions/cm^2). However, also with this dose, the switching field is noticeably reduced compared with the pristine wire. From these results, the lowest cumulative dose applied (9.44×10^{13} ions/cm^2) appears to be the most effective for defining the ANC. The measured reduction can be attributed to the strong reduction in the local effective anisotropy resulting in a drop in the switching field. With the obtained results, it was possible to reduce the switching field by 14.5 mT and control the position of the nucleation point, which is enough to enable logic computation with nanomagnets by means of dipolar coupling. The error bars in Figs. 3 and 4 represent the standard deviation computed over different repetitions to take into account the stochasticity introduced by the temperature.

B. Logic Device

Nanomagnets with perpendicular anisotropy, coupled by means of dipolar interaction, can be a promising alternative to traditional computing for high energy efficiency operations for the possibility to stimulate a great number of devices with a single magnetic stimulus generating a great number of parallel computations. So far, different materials such as Co/Pt and Co/Ni and different device architectures have been studied to make this computational approach faster and more efficient [9], [11], [16]. To enable logic operation with nanomagnets, three conditions have to be fulfilled. First, it is required a noticeable difference in the switching fields between inputs and outputs, with the inputs harder than the outputs. Second, there must be enough magnetic coupling among them to obtain a reliable logic behavior. Finally, the ANC position must be in the proximity of the zone subjected to the maximum coupling to obtain the maximum influence of the input magnets on the output. The last condition is also required to define the propagation direction of the information. In Section III-A, we showed experimentally that it is possible to obtain an ANC in the Ta/CoFeB/MgO stack and that the magnetic properties of the magnets can be tuned by controlling the amount of Ga^+ ions irradiation applied. The minimal device to prove that a material system can be used for computation is the inverter. To realize this operation, the test structures shown in Fig. 5(a) and (b) were fabricated. The shape of the fabricated structures, Fig. 5(c), is designed to emphasize the magnetic coupling. The input shape is designed to surround the output to increase the intensity of the demagnetizing field produced by the input magnet in the specific region, where the nucleation center of the output is going to be placed. The inversion operation can be obtained if the nucleation center is placed in an adequate position to be influenced by the strongest possible coupling from the input and a sufficient external field is applied to the structure.

Fig. 5(b) shows the layout of the test structures. To test different distances between the inputs and the outputs, the gap between the two islands of the inverter is increased starting from the bottom row. As shown in Fig. 5(b), the numbers on the left refer to the nominal dimensions of the gap in nm between the input and the output. All the tested structures were fabricated with a width of 100 nm at the initial part of the output. This region, the closest to the input, is the one hosting the ANC. Fig. 5(a) shows an optical image of the patterned structures. The irradiation pattern used to generate the ANC is a square 50 nm wide, placed at the left edge of the output. The inverters were irradiated in two steps. A first areal irradiation over the whole structure with a low irradiation dose and a second stronger local irradiation on the output to generate the required ANC. The picture in Fig. 5(c) reports a zoomed version of the inverter mask where it is possible to observe the ANC irradiation scheme. Due to the required precision for the placement of the ANC and possible misalignment during the FIB operation, four ANCs were placed for each inverter to increase the chance of generating an ANC in the output, the region subjected to the highest field.

The ion doses used for the areal irradiation and the ANC creation were obtained from the results found in the irradiation study performed on the wires shown in Section III-A. In particular, for the areal irradiation, the structures were irradiated with a dose of 2.57×10^{13} ions/cm^2. In the second step, the outputs were irradiated in the ANC region with an additional dose of 8.5×10^{13} ions/cm^2. In the ANC irradiation step, the cumulative ions' dose applied is higher than the optimal one found in the previous analysis due to an oscillation in the beam current. Besides not being in the optimal point, the final dose of 1.1×10^{14} ions/cm^2 generates a sufficient reduction in the switching field to create an effective ANC, as shown in Fig. 4 and was used for the inverter devices analysis.

Fig. 5(d) and (e) shows the result of the patterning process, imaged by the WMOKE and by the AFM, respectively. In image 5(d), the black color represents the up magnetization direction, proving that the structures were still perpendicularly

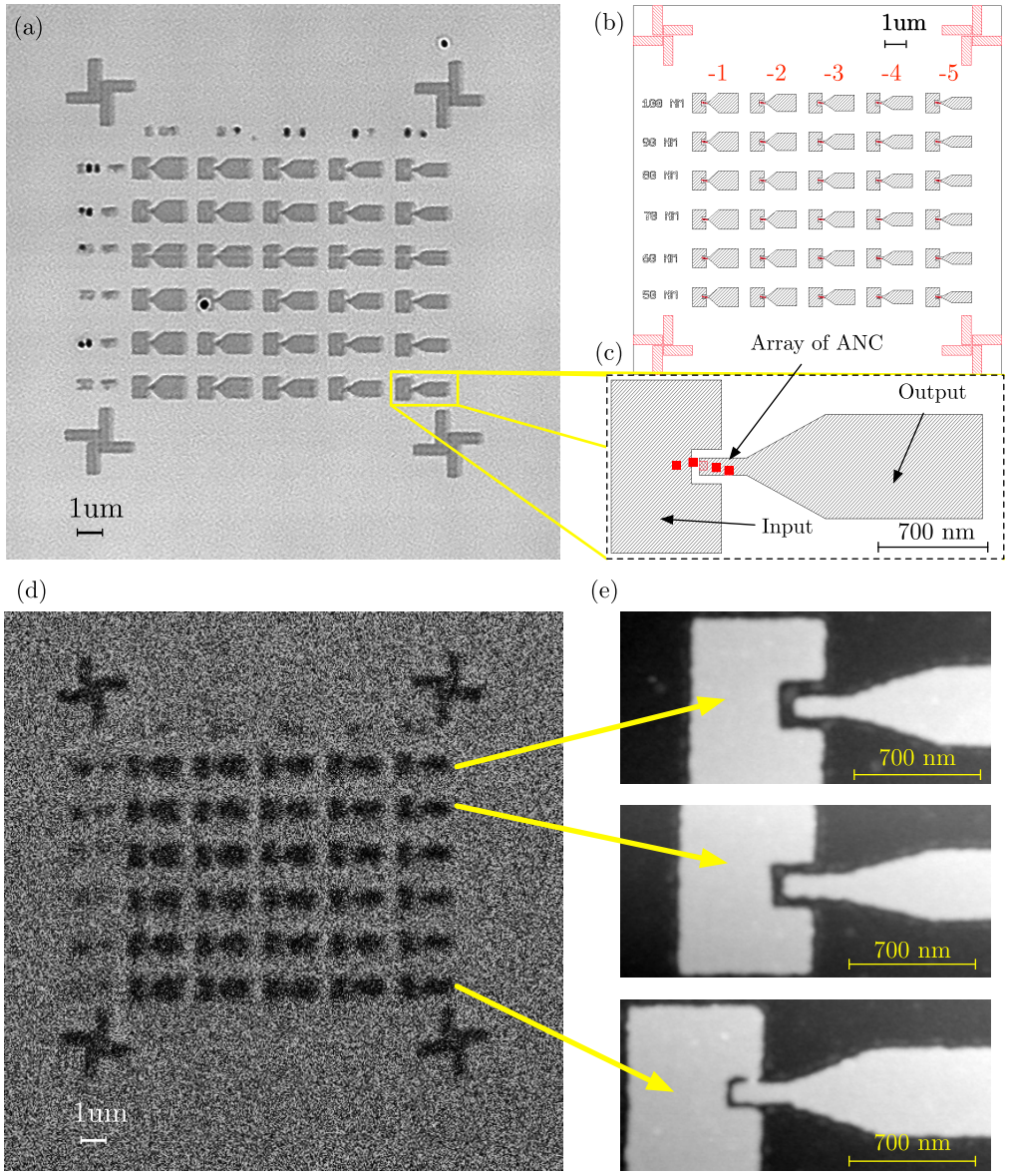

Fig. 5. (a) Optical image of the fabricated inverters. (b) Complete FIB lithography mask. (c) Zoom of an inverter showing the ANC irradiation scheme. (d) WMOKE image of the box containing 30 inverters saturated with 50 mT before areal irradiation. (e) AFM images of the inverters with a gap of 100 nm (top), 90 nm (central), and 80 nm (bottom).

magnetized after sample processing. AFM measurements of the inverters were performed to determine the real dimensions of the gaps and verify the complete separation between the input and output magnets. Fig. 5(e) shows three exemplary measurements with different gaps. As not all the inverters have a complete gap, only those in which the input and the output show a net separation are taken into account for the study.

The switching field of the output islands is measured with different conditions of the input magnets. The switching behavior of this part of the inverter is measured starting from two different configurations to compute the magnetic coupling between the input and the output and evaluate the correct placement of the ANC on the output island. In the first configuration, named "supported," the input and the output start from the same negative saturated state and are then subjected to positive external fields. In this regime, the demagnetizing field of the input supports the reversal of the output magnetization. The mean external field required to reverse the output magnetization, if the ANC is correctly placed, is then lowered with respect to its natural coercive field. In the second condition, named "prevented," the input and the output are saturated with opposite magnetization directions, respectively, negative and positive, and an external field is applied in the negative direction. In this configuration, the demagnetizing field of the input prevents the magnetization reversal of the output. Therefore, the external field required to reverse the output magnetization is expected to be higher compared with the switching field of the outputs without the influence of the inputs. The shift between the natural switching fields of the output magnet and the one with the influence of the input defines the magnetic coupling of the two magnets.

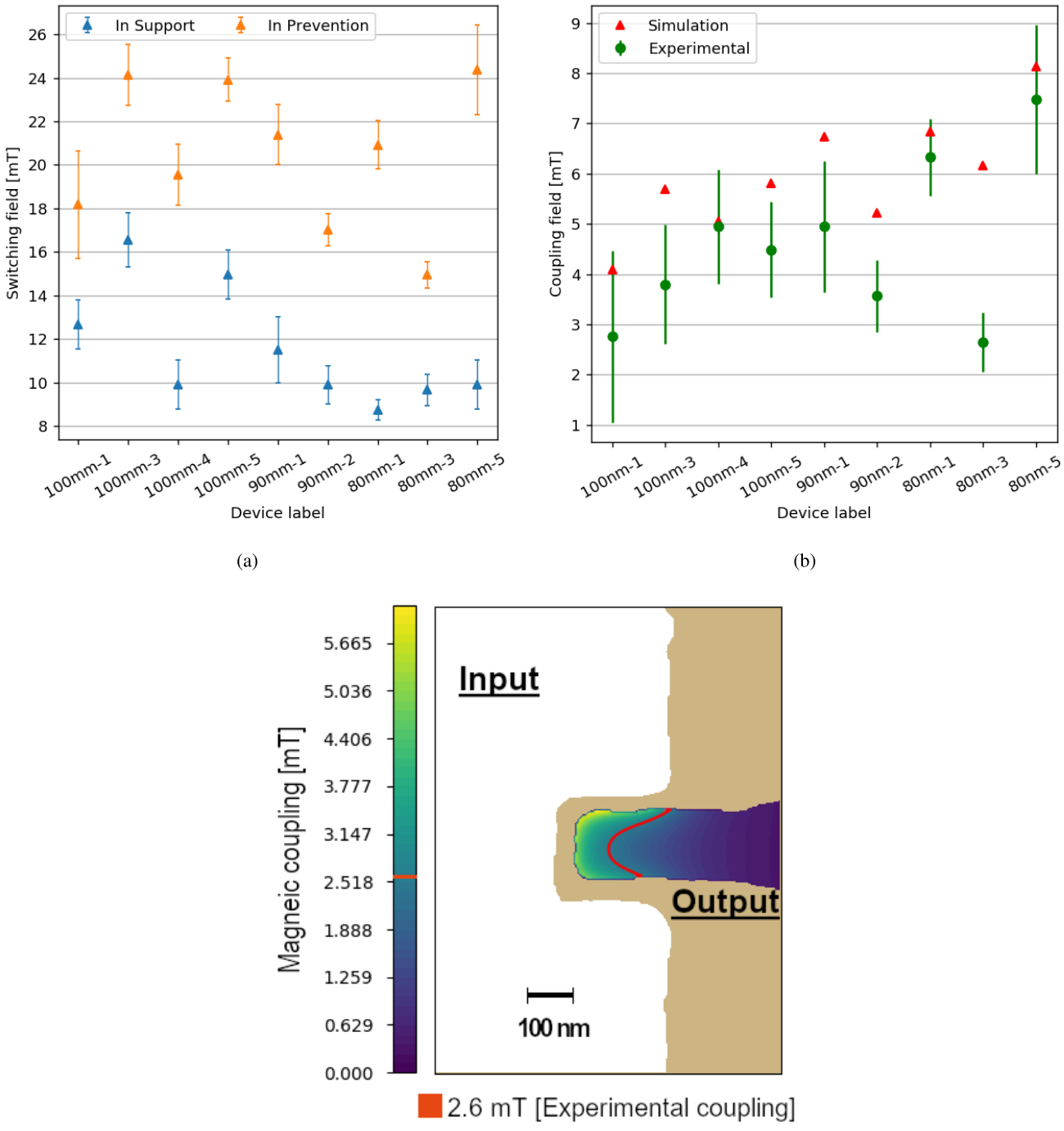

Fig. 6. (a) Experimental switching field in prevented and supported configuration. (b) Input–output magnetic coupling computed from experimental data and micromagnetic simulation of the devices measured by AFM. (c) Coupling extracted from micromagnetic simulation of device 80 nm^{-3}. The red line is the computed magnetic coupling correspondent to the coupling value measured experimentally for the device.

Experimentally, this value can be computed as

$$C = \frac{|H_P| - |H_S|}{2} \tag{1}$$

where H_P is the mean output switching field registered in the prevented initial configuration, and H_S is the mean output switching field registered in the supported initial configuration. Fig. 6(a) reports the switching field measured in the supported and prevented cases. In Fig. 6(b), the computed dipolar coupling is shown. As expected, with the reduction in nominal distances from 100 to 80 nm, the maximum coupling registered increases in magnitude. In the best case, with a nominal distance of 80 nm, a value of 7.25 mT was measured. As can be seen from Fig. 6(b), a visible variation among the inverters is present. As already shown in the AFM images, Fig. 5(e), the structures differ from the

nominal geometry, and this can induce a variation in the maximum achievable coupling. In addition, another relevant parameter is the magnetic field generated by the input at the ANC: therefore, its position is crucial to determine the strength of the coupling. The nucleation process originates from that point, so the ANC must be placed as close as possible to the input to be subjected to the maximum coupling. Therefore, successful reversal depends directly on the strength of the magnetic field generated by the input magnet in the position in which the nucleation center is defined. The not uniform shape introduced by the used etching process and possible misalignment of the FIB irradiation with respect to the patterned structure are considered the most important factors that determine this variation. To better appreciate the effect of these factors on the real inverters, the devices are studied by means of micromagnetic simulations starting from the AFM measurements of the devices. The inverters are simulated by means of Mumax3 software [17], [18]. The simulations were carried out at 0 K. The saturation magnetization has been set to 8.3×10^5 Am^{-1} as reported in [10] for a stack with the same composition. To evaluate the magnetic coupling of the real devices, the demagnetizing field produced by the input was evaluated in the zone occupied by the output. The maximum value registered from this simulation was then taken as the value for the maximum achievable coupling. The results of the evaluation are reported in Fig. 6(b) with red triangles. The trend of the coupling obtained experimentally is respected in most of the simulated structures. In particular, the structures that experimentally showed the strongest couplings are also the ones that in the simulation showed the highest performance. This shows that the simulation is able, starting from the AFM images of the devices, to predict with a margin the achievable performance of the device unless the effect of thermal fluctuation. In particular, the inclusion of the thermal fluctuation is expected to lower the obtained coupling due to the support in both the prevented and supported cases of the switching of the output magnet. It is important to note that in some devices, the coupling predicted from simulation differs from the experimental value of more than 1 mT. As an example, the 80 nm^{-3} device shows experimentally a coupling of 2.6 mT with respect to a predicted coupling of 6.17 mT. This suggests that in this particular device, the ANCs were placed in a position at least 120 nm far from the rightmost edge of the input where the magnetic coupling is stronger. In accordance with the theory and as shown in the literature [16], this experiment shows that the optimal distance for the strongest coupling between I/O nanomagnets is the smallest possible one. However, as we can clearly see in Fig. 6(b) from the not-monotonically increase in the coupling field with the gap reduction, the more the structures become small and complex, the more the alignment becomes challenging. As shown in Fig. 6(c), the alignment of the ANC with respect to the structure is a crucial parameter to obtain a strong coupling, and the optimal distance heavily depends on it. Precision in the order of a tenth of nanometers is therefore required to obtain devices with uniform performance. In addition, it is important to note how optimized strategies for the ANC placement, like the placement of multiple ANCs to reduce the chance of missing the best spot for nucleation, can be effective to reduce the effect of ANC placement variations.

IV. Conclusion

With this article, we demonstrated that Ta/CoFeB/MgO films can be good candidates to perform logic operations based on magnetic dipolar coupling. Thanks to ion irradiation, it is possible to tune the magnetic properties of the nanostructures both by increasing and decreasing the effective anisotropy. The results of the irradiation study are, for the first time, implemented to create working logic devices based on Ta/CoFeB/MgO and show that with FIB irradiation we can not only control the nucleation point but also set the signal propagation direction and enable logic computation in nanomagnets with magnetic interactions. The coupling measured in the patterned devices is strong enough and allows to perform simple logic operations even if it is lower than the one obtained with Co/Pt multilayer stacks. However, the lower thickness (less than 10 nm) and the lower switching field (reduced down to 10 mT after the ANC creation) of the Ta/CoFeB/MgO nanomagnets make the technology appealing from the power consumption perspective, with a halved switching value with respect to the upper boundary for clocking fields targeted in [9]. Despite the high variability introduced by the fabrication process, we were able to reach a coupling field up to 7.25 mT and modify the switching behavior of the magnets up to 14.5 mT. In addition, we showed the impact of ANC position on the output magnet and its importance in maximizing the coupling strength. The findings of this research pave the way for further development of the technology, such as the investigation of the role of dipole–dipole interaction in more complex systems and array of devices.

Appendix A
Micromagnetic Simulations

We exploited micromagnetic simulations performed with the GPU-accelerated software package Mumax3 [17] to study and optimize the nucleation center position and support the experiments. We considered a 1 nm thick Ta/CoFeB/MgO/Ta with PMA. In the first part, we characterized the most effective layout in terms of ANC geometry and position, while in the second, we verified the correct operation of the inverter structure before proceeding with the real experiment. Both the simulations are carried on at $T = 0$ K. The thermal effects are not considered in these simulations as their addition is expected to influence in the same way all the presented results.

A. ANC Geometry and Position

The simulated structure is a wire with a length of 400 nm, a width of 80 nm, and a thickness of 1 nm (Fig. 7). The magnetic properties are listed in Table I.

The values of the magnetization saturation (M_s) and uniaxial anisotropy constant (Ku_{film}) are taken from [2] and are measured values from a sample with the same stack composition and process parameters to the one fabricated in this work. The damping constant (α) and the exchange stiffness (A_{ex}), instead, are taken from [19]. The discretization

Fig. 7. Simulated structures: (a) squared ANC (50 nm side) in the center; (b) squared ANC (50 nm side) at the border; and (c) circular ANC (56.4 nm diameter) at the border. The wire is 400 nm long, has a width of 80 nm, and it is 1 nm thick.

TABLE I
MAGNETIC PARAMETERS IMPLEMENTED IN THE SIMULATIONS

Parameter	Value	Unit of measure
M_s	$8.3 \cdot 10^5$	$\frac{A}{m}$
Ku_{film}	$5.6 \cdot 10^5$	$\frac{J}{m^3}$
Ku_{ANC}	$0.7 \cdot Ku_{film}$	$\frac{J}{m^3}$
α	0.015	-
A_{ex}	$2 \cdot 10^{-11}$	$\frac{J}{m}$

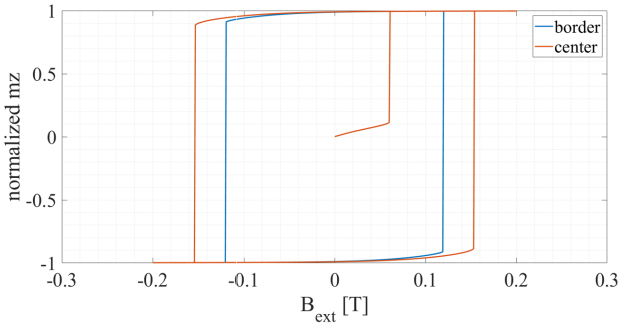

Fig. 8. Hysteresis comparison of a wire with the ANC placed at the border (blue curve) and at the center (red curve). Structures represented in Fig. 7(a) and (b).

of the sample is 2.5 × 2.5 × 1 n^{3}m. We assumed the magnet to be perfect, so grains and defects are not taken into account, being interested in a qualitative analysis of the impact of the geometry and position of the ANC. The first part of the simulations regards the position of the ANC. Two different layouts are simulated, the first, with the ANC in the center of the wire, and the second with the ANC in contact with the uppermost border (as shown in Fig. 7).

The difference in the switching behavior is investigated through a hysteresis analysis of the two layouts. These simulations are static, and the external field is varied in three steps, from 0 to 200 mT, then from 200 to −200 mT, and finally from −200 to 200 mT. The field is varied in step of 1 mT, and the z-component of the magnetization vector of the whole wire is acquired at each field value. Fig. 8 shows

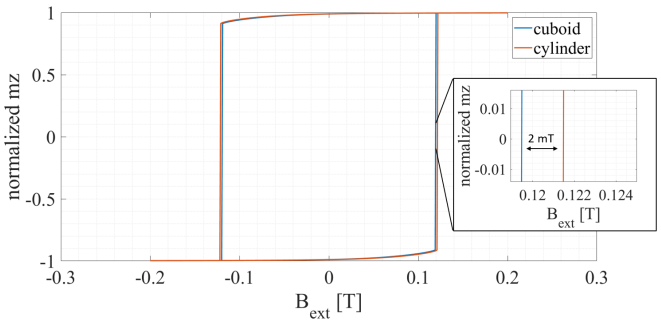

Fig. 9. Hysteresis in case of squared and circular ANC placed at the border. The simulated structures are shown in Fig. 7(b) and (c).

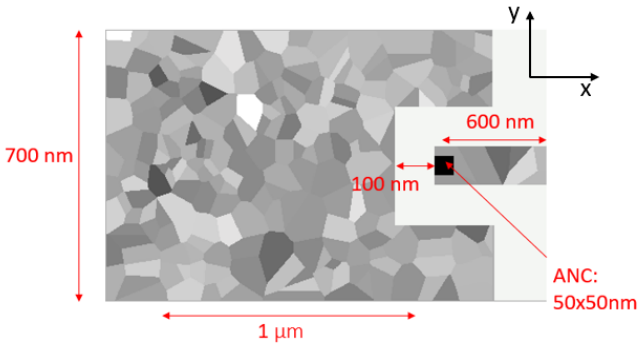

Fig. 10. Simulated structures: fork-like coplanar inverter.

the comparison of the computed hysteresis. With the ANC at the border, the switching occurs several mT lower (∼34 mT in this analysis) than the case in the center. This, although the maximum value of the demagnetizing field that helps the magnetization reversal, should be in the center of a magnet. The reason could be found in the fact that at the border, the magnetic moments tend to naturally turn faster at the edges. It is worth saying that these very high values of coercivity ($H_{c\text{-border}} = 120$ mT and $H_{c\text{-center}} = 154$ mT) are obtained due to the ideal assumptions discussed before.

The other question investigated in this simulation study is the possible impact of the shape of the ANC on the switching behavior of the magnet. Two structures are simulated, one with a squared ANC (50 × 50 nm) and the other with a circular ANC, with the same volume as the first (diameter = 56.4 nm). From the hysteresis in Fig. 9, a small difference of 2 mT is present between the two cases. In particular, the ANC with a square shape allows reaching lower switching fields. These simulations suggest that placing a squared ANC in contact with the border of the wire [Fig. 7(b)] can help reduce the switching field, maximizing the effect of the ANC with respect to other geometries, allowing to decrease the energy required to perform logic computation. The orientation of the squared ANC is not expected to play a major role in the efficiency of the ANC in the reduction in the switching field. In particular, no difference is expected in the case of the ANC centered in the magnet, while for one placed on the border, a different orientation can reduce the performance due to the reduced contact of the irradiated zone with the border of the magnet.

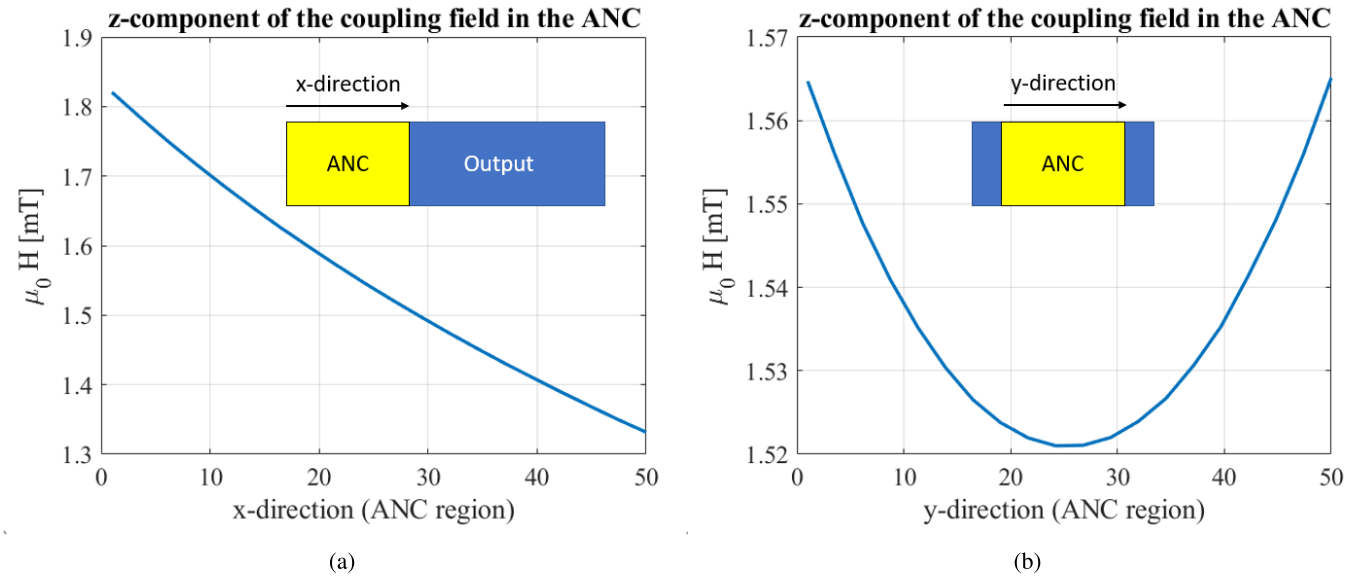

Fig. 11. z-component of the coupling field in the ANC region (input initial magnetization: $m_z = -1$): (a) along the ANC x-direction and (b) along the ANC y-direction.

The natural tilting of the magnetic moments at the edge of the sample can play an important role in helping the nucleation and expansion of the reversed domain. Further information can be found in [[10], Supplementary information].

B. Inverter Coupling Verification

The second part of the simulations has the goal of verifying the intensity of the dipolar field generated between two adjacent magnets and the possibility of performing an inversion operation. The simulated structure is similar to the one used in the experiments, and it is shown in Fig. 10. The gap between the input and the output is 100 nm and the ANC is a square of sides 50 nm, placed in contact with the leftmost border of the output, which is a wire 100 nm wide. The magnetic parameters are the ones presented in the previous simulations with the addition, in this case, of material grains (being interested in a more quantitative analysis with respect to Section A-A). The introduced random grains' structure has a nominal size of 15 nm and a maximum variation of Ku of 5% with respect to the nominal anisotropy constant. The presence of coupling is investigated either via minimization of the system energy and via dynamic Landau–Lifshitz–Gilbert (LLG) simulations. Through the minimization of the system energy, the z-component of the demagnetizing field generated from the input is derived in the region of the ANC, as shown in Fig. 11. Dynamic LLG simulations instead allow to verify the inversion operation, providing the switching field of the output when the input supports or prevents the switch and making it possible to derive from these results the value of the coupling field.

The results of the simulation are shown in Fig. 12. The magnetization of the output is initialized in the negative z direction ($m_z = -1$), and the input is initialized in both the directions to verify the intensity of the external field needed to switch the output magnetization in both the cases. During the simulations, a positive magnetic field is applied along z to switch the magnetic state of the output. In the first case, named supported case, the initial situation is the one in which input and output have the same magnetization in the negative direction, and due to the antiferromagnetic coupling, the output switch is favored by the stray field generated by the input. This makes it possible to invert the information encoded in the input magnetization. In the second simulated configuration, named prevented case instead, the input and output have opposite magnetization directions, and an inversion of the input signal is already present in the initial state. So, a switch of the output is counteracted by the stray field of the input. From the above simulation, the coupling is computed as $(H_p - H_s)/2$, where H_p and H_s represent the lowest field that allows the switch of the output, respectively, in the supportive case and in the prevented case. From the simulations, the lowest switching field was found in the supported case, and it is equal to 99.4 mT, while in the prevented case the switching field is equal to 102.4 mT. The presence of a difference in values means that the coupling exists and its computed value from the above switching fields is equal to 1.5 mT. The granular structure used in the different simulations is exactly the same to correctly evaluate the coupling field produced by the input–output configuration. To better understand these results, the stray field distribution produced from the input in the output region is derived through static computation of the stray fields excluding the output influence. Fig. 11(a) shows the expected monotonic decrease in the coupling field along the x-direction (meaning that we are moving further and further away from the input). In Fig. 11(b), it is possible to appreciate the nonlinear behavior of the field, which presents its minimum at the center of the input aperture where the ANC should be placed to obtain the best performance in terms of input–output coupling.

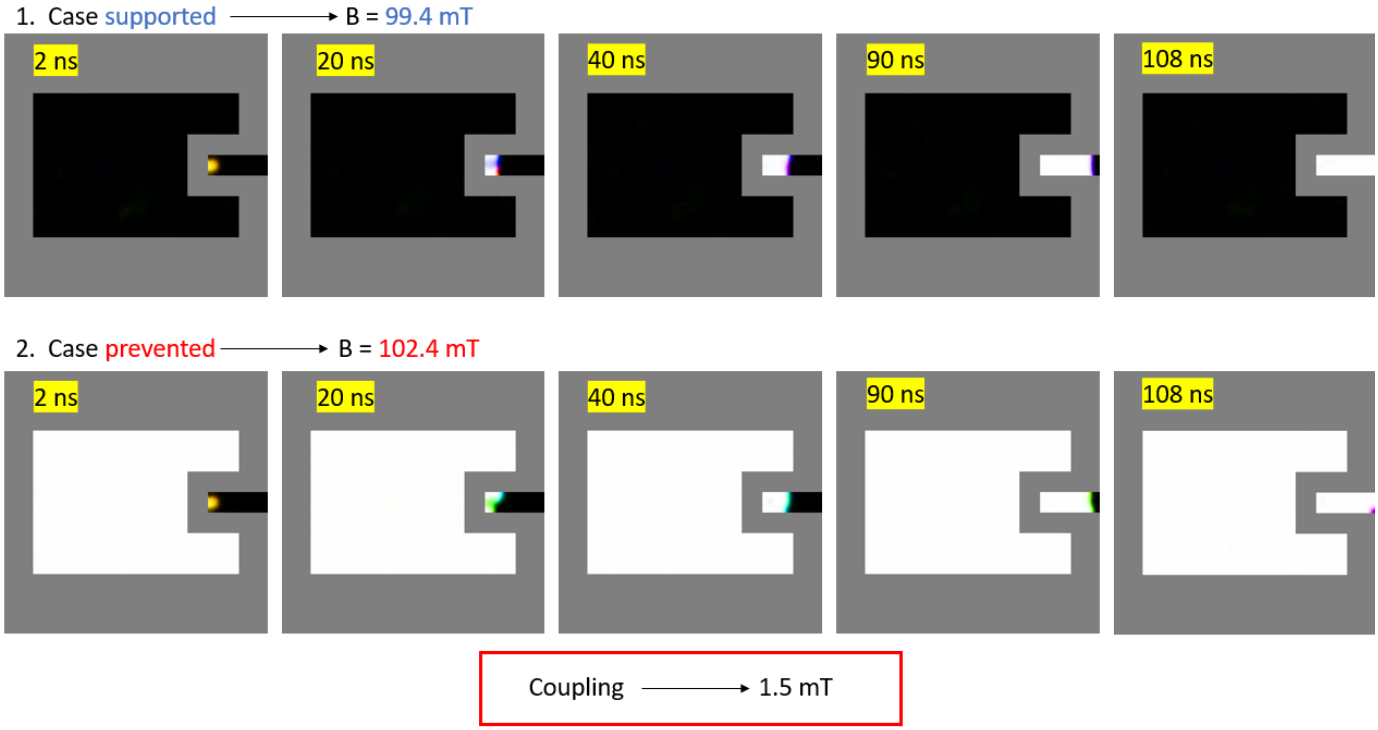

Fig. 12. Micromagnetic simulation of an inverter in the case in which the inversion is supported (upper row) and prevented (bottom row). The magnetic parameters of the structure are listed in Table I. The input has a fork-like structure to surround the ANC and maximize the coupling. The dimensions are 0.7×1 μm, the gap is 100 nm as the width of the output, and the ANC is a square of 50 nm side placed in contact with the left border of the output.

ACKNOWLEDGMENT

This work was supported in part by the LIFTT based on funds from the Compagnia di San Paolo, carried out as part of the Proof of Concept (PoC) Instrument initiative implemented by LINKS and in part by the Central Electronics and Information Technology Laboratory—ZEIT$^{\text{lab}}$.

REFERENCES

[1] S. Ota et al., "CoFeB/MgO-based magnetic tunnel junction directly formed on a flexible substrate," *Appl. Phys. Exp.*, vol. 12, no. 5, Apr. 2019, Art. no. 053001, doi: 10.7567/1882-0786/ab0dca.

[2] F. Riente, S. Mendisch, L. Gnoli, V. Ahrens, M. R. Roch, and M. Becherer, "Ta/CoFeB/MgO analysis for low power nanomagnetic devices," *AIP Adv.*, vol. 10, no. 12, Dec. 2020, Art. no. 125229.

[3] K. Garello et al., "SOT-MRAM 300 MM integration for low power and ultrafast embedded memories," in *Proc. IEEE Symp. VLSI Circuits*, Jun. 2018, pp. 81–82.

[4] F. Riente et al., "Controlled data storage for non-volatile memory cells embedded in nano magnetic logic," *AIP Adv.*, vol. 7, no. 5, May 2017, Art. no. 055910.

[5] I. Eichwald, S. Breitkreutz, J. Kiermaier, G. Csaba, D. Schmitt-Landsiedel, and M. Becherer, "Signal crossing in perpendicular nanomagnetic logic," *J. Appl. Phys.*, vol. 115, no. 17, May 2014, Art. no. 17E510, doi: 10.1063/1.4863810.

[6] G. Turvani, F. Riente, E. Plozner, M. Vacca, M. Graziano, and S. B. Gamm, "A pNML compact model enabling the exploration of three-dimensional architectures," *IEEE Trans. Nanotechnol.*, vol. 16, no. 3, pp. 431–438, May 2017.

[7] I. Eichwald, S. Breitkreutz, G. Ziemys, G. Csaba, W. Porod, and M. Becherer, "Majority logic gate for 3D magnetic computing," *Nanotechnology*, vol. 25, no. 33, Jul. 2014, Art. no. 335202.

[8] S. Breitkreutz et al., "1-bit full adder in perpendicular nanomagnetic logic using a novel 5-input majority gate," in *Proc. EPJ Web Conf.*, vol. 75, 2014, p. 5001, doi: 10.1051/epjconf/20147505001.

[9] S. Mendsich, V. Ahrens, M. Kiechle, A. Papp, and M. Becherer, "Perpendicular nanomagnetic logic based on low anisotropy Co/Ni multilayer," *J. Magn. Magn. Mater.*, vol. 510, Sep. 2020, Art. no. 166626. [Online]. Available: https://www.sciencedirect.com/science/article/pii/S0304885319330550

[10] S. Mendisch et al., "Controlling domain-wall nucleation in Ta/Co-Fe-B/MgO nanomagnets via local Ga^+ ion irradiation," *Phys. Rev. Appl.*, vol. 16, no. 1, Jul. 2021, Art. no. 014039, doi: 10.1103/PhysRevApplied.16.014039.

[11] S. Breitkreutz et al., "Experimental demonstration of a 1-bit full adder in perpendicular nanomagnetic logic," *IEEE Trans. Magn.*, vol. 49, no. 7, pp. 4464–4467, Jul. 2013.

[12] X. Zhao et al., "Enhancing domain wall velocity through interface intermixing in W-CoFeB-MgO films with perpendicular anisotropy," *Appl. Phys. Lett.*, vol. 115, no. 12, Sep. 2019, Art. no. 122404, doi: 10.1063/1.5121357.

[13] T. Devolder et al., "Irradiation-induced tailoring of the magnetism of CoFeB/MgO ultrathin films," *J. Appl. Phys.*, vol. 113, no. 20, May 2013, Art. no. 203912.

[14] L. Herrera Diez et al., "Controlling magnetic domain wall motion in the creep regime in He^+-irradiated CoFeB/MgO films with perpendicular anisotropy," *Appl. Phys. Lett.*, vol. 107, no. 3, Jul. 2015, Art. no. 032401.

[15] L. H. Diez et al., "Enhancement of the Dzyaloshinskii–Moriya interaction and domain wall velocity through interface intermixing in Ta/CoFeB/MgO," *Phys. Rev. B, Condens. Matter*, vol. 99, no. 5, Feb. 2019, Art. no. 054431, doi: 10.1103/PhysRevB.99.054431.

[16] P. Zhou et al., "Multilayer nanomagnet threshold logic," *IEEE Trans. Electron Devices*, vol. 68, no. 4, pp. 1944–1949, Apr. 2021.

[17] A. Vansteenkiste, J. Leliaert, M. Dvornik, M. Helsen, F. Garcia-Sanchez, and B. Van Waeyenberge, "The design and verification of MuMax3," *AIP Adv.*, vol. 4, Apr. 2014, Art. no. 107133, doi: 10.1063/1.4899186.

[18] J. Mulkers, B. Van Waeyenberge, and M. V. Milošević, "Effects of spatially engineered Dzyaloshinskii–Moriya interaction in ferromagnetic films," *Phys. Rev. B, Condens. Matter*, vol. 95, no. 14, Apr. 2017, Art. no. 144401, doi: 10.1103/PhysRevB.95.144401.

[19] R. Tomasello, E. Martinez, R. Zivieri, L. Torres, M. Carpentieri, and G. Finocchio, "A strategy for the design of skyrmion racetrack memories," *Sci. Rep.*, vol. 4, p. 6784, Oct. 2014.

Open Access funding provided by 'Politecnico di Torino' within the CRUI CARE Agreement